Received: 12 June 2023 | Revised: 8 January 2024 | Accepted: 9 January 2024

DOI: 10.1002/qj.4660

Quarterly Journal of the Royal Meteorological Society RMetS

RESEARCH ARTICLE

The use of idealised experiments in testing a new convective parametrization: Performance of CoMorph-A

Sally L. Lavender[1,2] | **Alison J. Stirling**[2] | **Michael Whitall**[2] | **Rachel A. Stratton**[2] | **Chimene L. Daleu**[3] | **Robert S. Plant**[3] | **Adrian Lock**[2] | **Jian-Feng Gu**[3,4]

[1]Centre for Applied Climate Sciences, University of Southern Queensland, Toowoomba, Queensland Australia

[2]Met Office, Exeter, UK

[3]Department of Meteorology, University of Reading, Reading, UK

[4]Key Laboratory of Mesoscale Severe Weather, Ministry of Education, and School of Atmospheric Sciences, Nanjing University, Nanjing, China

Correspondence
S. L. Lavender, Centre for Applied Climate Sciences, University of Southern Queensland, Toowoomba, Australia.
Email: sally.lavender@usq.edu.au

Funding information
Natural Environment Research Council, Grant/Award Number: NE/N013743/1

Abstract

CoMorph is a new mass-flux convection parametrization under development at the Met Office designed for use within the Unified Model and its successor model, LFRic. Use of a three-dimensional idealised model enables controlled tests of the performance of the scheme across different regimes. This includes the interaction between the physical parametrizations and the resolved dynamics, allowing study of the emergent organisation of convection on the resolved scale. A selection of well-known cases is revisited here, with the purpose of documenting the extent to which CoMorph captures a range of important, but challenging, behaviour such as the diurnal cycle and sensitivity to tropospheric moisture. Simulations using CoMorph-A, a new physics package, that has been demonstrated to perform well at numerical weather prediction (NWP) and climate scales, are compared against the current global atmosphere configuration and high-resolution results. In addition to an entirely new convection scheme, the package of changes includes significant changes to the cloud, microphysics, and boundary-layer parametrizations. Recognising that CoMorph-A is the first version of a scheme that will continue to be substantially developed and to obtain good performance, compromises in tuning have had to be made. These idealised tests therefore show what works well in this configuration, and what areas will require further work. As such, it is quite a demanding testbed and could be viewed as some of the equipment required for a "convective playground".

KEYWORDS

climate models, cloud-resolving models, convection parametrization, diurnal cycle, idealised modelling

1 | INTRODUCTION

Convective clouds act to transport heat, moisture and mass upwards, fuelled by the latent heat release of condensing water from rising air parcels. Since this motion cannot accurately be represented on the resolved model grid, a convection parametrization needs to represent the effects of this dynamical process by estimating its influence on the temperature, moisture and horizontal winds of the atmosphere, in addition to predicting the precipitation generated. The subsequent adjustment of the temperature profile by the resolved scale has an influence on the wider circulation patterns. As such, whether the convection scheme in a model adequately represents the spatial and temporal distribution of convective precipitation and diabatic heating has implications not only for local precipitation accumulations but also for global circulation patterns through convective–dynamical coupling.

The Met Office Unified Model (UM: Brown et al., 2012) is used extensively across the world with partnership institutions including the Australian Bureau of Meteorology, the National Centre for Medium Range Weather Forecasting (NCMRWF) in India and the Meteorological Service Singapore. For over 30 years, the Met Office convection scheme has been based on the mass-flux approach of Arakawa and Schubert (1974), in which the role of the convection scheme is to stabilise atmospheric profiles via the removal of CAPE (convectively available potential energy) through subsidence within a grid column. The existing scheme, based on Gregory and Rowntree (1990), lacks much of the structural flexibility required to address systematic biases generated by convection in the UM (e.g. Walters et al., 2019). To address this, a new convection scheme, CoMorph, has been developed (see Whitall et al. (2022) for full details). Whilst still a bulk mass-flux scheme, CoMorph removes previously hardwired structural assumptions such as initiation from a predetermined cloud-base height and the use of separate schemes for shallow, deep and mid-level convection which must be pre-diagnosed. CoMorph has been written in a way that allows the inclusion of additional physics, and couples more fully and consistently to other physics components of the model (see Section 2.2). A package of changes called CoMorph-A has been released and simulations in a full global circulation model (GCM) have shown the positive impact of including this package in the GCM (A. Lock, submitted work). These benefits include a reduction in radiative flux biases across the tropics, improvements in tropical and extratropical cyclone statistics, strengthening of the Madden–Julian Oscillation (MJO) and other tropical waves as well as improvements in overall scores in numerical weather prediction trials.

It is common to use single-column models (SCMs) alongside convection-resolving models (CRM) or large-eddy simulation (LES) together with field observations whilst developing and testing parametrizations (e.g. Lenderink et al., 2004; Grabowski et al., 2006; Couvreux et al., 2015). However, SCMs are unable to capture feedbacks between subgrid- and grid-scale processes which can lead to different behaviour than the full GCM. For example, SCM cases have been successfully used to develop improvements to convective parametrizations to represent the diurnal cycle of convection over land (e.g. Rio et al., 2009) but additional modifications may be needed to perform well in the GCM due to interactions not originally exposed by the SCM (e.g. Rio et al., 2013). In a recent study, Hwong et al. (2022) found that as convection becomes more organised, there are larger differences in results between one- and three-dimensional (3D) simulations. Although the UM SCM has been used extensively during development of CoMorph, this study uses the 3D idealised UM. While still being substantially cheaper to run than the full GCM, this enables controlled tests of the interaction between the physical parametrizations and the resolved dynamics, enabling more comprehensive testing of the scheme, including the emergent organisation of convection on the resolved scale.

A selection of well-known cases is revisited here, with the purpose of documenting the extent to which CoMorph-A captures a range of important, but challenging, behaviour. These idealised cases have the advantage that they can be accompanied by high-resolution analogues, where the convection is well captured by the resolved grid. Many of these cases were originally designed for use in an SCM for testing parametrizations over a grid box of order 100–200 km; however, the UM, along with many other GCMs, is now routinely run at much higher resolutions of order of 10–50 km. Using the idealised UM configured to use the same physics as in the full GCM allows some exploration of how the model will behave at these higher resolutions. Results from a coarser resolution (10 km and lower) model set-up with parametrized convection (with and without CoMorph-A) are presented alongside high-resolution (250 m or higher) CRM results. CoMorph has around 30 tuneable parameters, so many different versions have been tested in the development of a package that performs well operationally. Recognising that CoMorph-A is the first version of a scheme that will continue to be substantially developed, compromises in tuning have had to be made in order to obtain good performance. These idealised tests evaluate where this configuration performs well and identifies any deficiencies that require further work. This testbed is designed to serve as a reference for others to replicate, and could be viewed as some of the equipment required for a

"convective playground"; a platform to enable testing of convection parametrizations with differing levels of complexity, from simple idealised tests through to comparisons with field campaigns.

The following section describes the idealised UM and details of the CoMorph-A package of changes. Section 3 gives an overview of multiple experiments and documents the performance of CoMorph-A. The results are summarised in Section 4.

2 | MODEL EXPERIMENTS

2.1 | Model overview

The atmospheric model used is version 12.1 of the UM. In the idealised configuration the model has bicyclic boundary conditions over a limited area domain on a flat, Cartesian grid.

The full science set-up with parametrized convection is based on the current operational global atmosphere and land configuration, GAL8. This configuration is based on that described by Walters et al. (2019) with updates to some of the physics. These include the addition of a drag package, changes to the boundary-layer scheme to improve representation of shear-driven boundary layers as well as the numerical stability of stable boundary layers, and a new riming parametrization in the large-scale precipitation scheme. For the control run (CTRL) using GAL8 as officially defined, that is with the current UM convection scheme, there have been significant changes to the existing convection scheme including the use of a prognostic entrainment rate to allow some memory of recent convection (Willett & Whitall, 2017). The additional changes in replacing the convection scheme with CoMorph-A are detailed in Section 2.2.

For the CRM with only explicit convection, the tropical regional atmosphere configuration, RAL2-T, is used as described in detail by Bush et al. (2023) but using the Smith (1990) cloud parametrization scheme and the same higher-order interpolation scheme for dry potential temperature and moisture. Tests have shown benefits of using the Smith (1990) diagnostic cloud parameterization scheme, as in the RAL2-M configuration (Bush et al., 2023) instead of the PC2 scheme (Wilson et al., 2008) when running at sub-km resolutions. Additionally, the Fountain Buster scheme is used which modifies the semi-Lagrangian advection scheme to address local conservation errors caused by unrealistically intense updraughts. Unless specified in the text, updraught mass fluxes from the CRM are calculated over buoyant cloudy updraughts whereby sub-grid velocity is upwards relative to the layer mean ($w' > 0\ \mathrm{m{\cdot}s^{-1}}$), cloudy points are defined by a cloud condensate mixing ratio greater than 1×10^{-5} ($\mathrm{kg{\cdot}kg^{-1}}$) and are positively buoyant relative to the layer mean ($\theta_v' > 0$).

A selection of idealised experiments has been used to develop and test the performance of CoMorph-A. Rather than provide details of all the idealised experiments here, these are described in Table 1 and the relevant results section where they are first mentioned. The reader is directed to the original papers for full details but any divergence from the original experiments is outlined. Where available, the results are compared against the CRM and previously documented results and observations.

2.2 | The CoMorph-A physics package

The CoMorph convection scheme is detailed in Whitall et al. (2022). Here we briefly describe some of the fundamental components of the scheme and detail differences from the existing scheme.

- In the previous scheme, updraughts are prescribed from a predetermined cloud-base height with a CAPE closure assumption to calculate the mass flux at cloud base. In CoMorph, mass flux is allowed to initiate independently from all heights where there is local vertical instability (dry-statically unstable layers such as near a heated surface, or moist stratiform cloud layers which become moist-unstable layers such as from large-scale cloud). When convection triggers from non-cloudy model-levels, the cloud-base height emerges from the scheme when the modelled bulk plume rises high enough to reach saturation. The amount of mass initiated is set to depend on the vertical instability, and this is effectively the "closure" for the scheme. The cloud-base mass flux then becomes determined by the balance of entrainment versus detrainment in the layer below cloud base.
- Entrainment rate scales with the inverse "parcel radius", which is based on a boundary-layer turbulence length-scale in the parcel's source-layer. The parcel radius in CoMorph-A is also scaled by an ad-hoc function of the previous time-step precipitation rate allowing a crude representation of increased organisation of convection by precipitation-driven cold pools.
- The detrainment rate is based on a power-law probability distribution function of in-plume buoyancy and other properties, with the core (lower entrainment rate) and mean properties of the plume treated separately. The ascent terminates at the level at which the parcel

TABLE 1 Summary of the experiments used in this article to evaluate the performance of CoMorph-A.

Section	Case title	Original reference	Domain (and resolution)	Interactive radiation?	Additional details	Scientific rationale
3.1. Mean state	RCE	Wing et al. (2018)	GA: $200 \times 200\ km^2$, $6000 \times 400\ km^2$ (10 km) CRM: $200 \times 200\ km^2$ (200 m)	Yes	SST = 300 K	Analysis of the mean-state and organisation of convection under radiative–convective equilibrium (RCE)
3.2 Sensitivity to tropospheric humidity	EUROCS	Derbyshire et al. (2004)	Multiple – see text	No	Relax (1 hr time-scale) to theta, wind and relative humidity profiles. Four different humidity profiles	Examining the moisture–convection relationship, shown to be important for simulating the MJO.
3.3 Diurnal cycle	Shallow ARM	Brown et al. (2002), Lenderink et al. (2004)	GA: $160 \times 160\ km^2$ (10 km) CRM: $160 \times 160\ km^2$ (100 m)	No	Prescribed surface fluxes, geostrophic wind of $(u, v) = (10, 0)\ m \cdot s^{-1}$.	Development of shallow cumulus over land with no transition to deep convection.
	AMMA	Couvreux et al. (2012, 2015)	GA: $100 \times 100\ km^2$ (10 km) CRM: $100 \times 100\ km^2$ (100 m)	No	Prescribed surface fluxes and temperature, moisture and vertical velocity tendencies	Large amplitude diurnal cycle with deep, dry boundary layer. Transition from shallow to deep convection.
	Deep ARM	Guichard et al. (2004)	GA: $100 \times 100\ km^2$ (10 km) CRM: $100 \times 100\ km^2$ (200 m)	No	Prescribed surface fluxes and temperature tendencies. Relax to zero wind	Idealised diurnal cycle case representing transition from dry to shallow to deep convection. Forced with the same cycle over 10 days.
3.4 Memory in diurnal cycle	As above (Deep ARM)	Daleu et al. (2020)	As above		As above	Quantifying the memory of the system in terms of the development of convection being influenced by previous convection.
3.5 Multi-day tropical case	TWP-ICE	Fridlind et al. (2012)	GA: $200 \times 200\ km^2$ (10 km), CRM: $200 \times 200\ km^2$ (100 m)	Yes	SST = 302.15 K, nudging of horizontal winds, moisture and temperature	Performance when simulating convective systems over multiple days. A well-documented case with interactive radiation.
3.6 Inland propagation and nocturnal convection	Island case	N/A	GA: $1200 \times 300\ km^2$ (10 km), CRM: $1200 \times 300\ km^2$ (250 m)	Yes	Island 300 km in x-dimension, real, flat, sandy land surface with plenty of moisture initially. $u = 0\ m \cdot s^{-1}$ and $u = 5\ m \cdot s^{-1}$	A newly developed case based on an island in the maritime continent to examine the initiation of convection by sea-breeze circulation and propagation of convection.
3.7 Convective momentum transport	Cold-air outbreak	Kershaw and Gregory (1997)	GA: $200 \times 200\ km^2$ (10 km), CRM: $200 \times 200\ km^2$ (100 m)	No	Prescribed, constant surface fluxes. $u = 0\ m \cdot s^{-1}$ and v linearly varies from $0\ m \cdot s^{-1}$ at the surface to $10\ m \cdot s^{-1}$ at 6 km	Sensitivity to different parametrizations of convective momentum transport.

core is negatively buoyant. This detrainment calculation also uses an implicit method to ensure it evolves smoothly over successive time steps.

- CoMorph includes a microphysics parametrization allowing formation of different hydrometeors within the parcel and allows the parcel and detrained air to remain supersaturated with respect to ice. All convectively generated precipitation is passed on the model-level where it falls out of the parcel to the "large-scale" microphysics scheme, which then simulates the fall to the surface, evaporation, melting, etc. To aid coupling between CoMorph and the large-scale microphysics at coarse resolution, both schemes update a prognostic precipitation fraction, so that convection can modify rain mass and area fraction consistently.
- CoMorph represents convective momentum transport (CMT) by transporting the zonal and meridional wind components within the bulk plume and allowing the exchange of momentum between the plume and environment with a parametrization of the horizontal pressure gradient force based on a quadratic drag law.

Compared to the previous UM convection scheme, CoMorph is much more closely coupled to the model's boundary layer, large-scale microphysics and prognostic cloud schemes, and modifications to all four schemes have been required to ensure they operate consistently together. The improved coupling between CoMorph and the resolved dynamics enables organised convective structures to develop over a range of scales.

3 | FOCUSSED TESTING OF COMORPH-A

In this section we focus on the performance of CoMorph-A in a range of different experiments targeting different model behaviours. An overview of all the test cases is given in Table 1 along with a summary of the rationale for selection of these cases. Since many of these cases are based on field campaigns, where the large-scale forcings have been observed/evaluated for specific areas, the domain sizes are chosen to be the same as those original cases. Where the original domain was smaller than $100 \times 100\,\mathrm{km}^2$ this has been increased to allow large-scale circulations to form in the parametrized cases. In cases where the domain size is 100–200 km^2, the runs have been repeated to check for any domain dependence. In all cases a discussion of the CRM results compared to other high-resolution results will be discussed and, where appropriate, plots are shown in a form that can be directly compared with earlier papers describing the case.

3.1 | Modelled mean state

To give an idea of the mean state, radiative–convective equilibrium (RCE) experiments were performed based on the RCEMIP set-up (Wing et al., 2018) with a sea-surface temperature of 300 K. The simulations are run for 100 days, reaching equilibrium after 20 days. The original RCEMIP CRM simulations show a large range of results. Figure 1a–c show profiles of potential temperature, relative humidity and updraught mass flux averaged over the final 70 days of the simulation. The parametrized runs have a warmer troposphere and higher altitude inversion than the CRM, leading to a higher termination of the updraught mass flux. CoMorph-A has a slightly warmer mid- to upper troposphere than CTRL and both parametrizations have a sharper inversion at cloud top than the CRM, with CoMorph-A slightly sharper than CTRL, possibly due to the current lack of representation of overshoots that would smooth out the inversion.

Consistent with other model results in Wing et al. (2020), the mid-tropospheric humidity in the parametrized runs is much lower than in the CRM where it remains above 75% in both simulations and becomes supersaturated with respect to ice above 8 km. This may suggest not enough detrainment in the plume formulation in both parametrizations. The CRM has a higher mass flux near cloud base and in the mid-troposphere but terminates at a lower altitude than both CTRL and CoMorph-A. CoMorph-A is drier than CTRL in the low to mid-troposphere with a resulting smaller mass flux.

A snapshot of the surface precipitation from day 50 of the 200 m CRM, CTRL and CoMorph-A simulations are shown in Figure 1d–f. Both parametrized runs show some aggregation of convection that is not so evident in the CRM simulation. The degree of aggregation in each simulation is quantified by calculating the subsidence fraction (f_{sub}), the fraction of the domain where there is subsidence, as in Wing et al. (2020) using daily 500 hPa vertical velocity averaged over $10 \times 10\,\mathrm{km}^2$ blocks (Figure 1g). The parametrized simulations were repeated using a domain of $6000 \times 400\,\mathrm{km}^2$ to check how the spatial organisation compares with the smaller domain. Using the large domain, the dependence of f_{sub} on the size of the blocks ($10 \times 10\,\mathrm{km}^2$ compared to $100 \times 100\,\mathrm{km}^2$ as used in the original study) was investigated and the values of f_{sub} were found to be similar. The values of f_{sub} in the CRM range from 0.5 to 0.6 compared to 0.7–0.8 in the parametrized runs, suggesting that there is greater organisation in the parametrized runs which may be excessive. However, these higher values of f_{sub} are within the same range as other CRM models analysed in RCEMIP (fig. 12 in Wing et al., 2020).

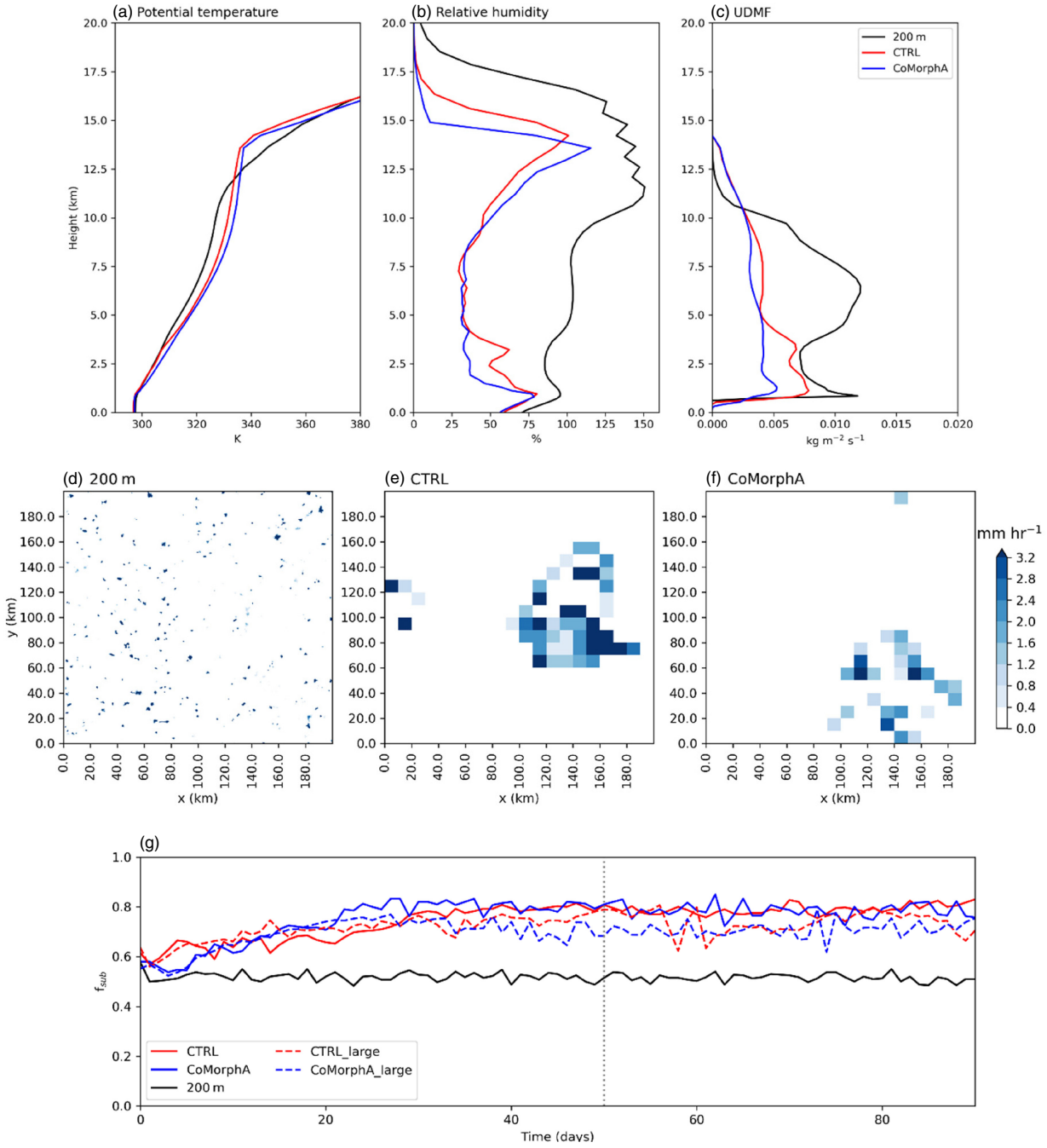

FIGURE 1 Radiative–convective equilibrium (RCE). Profiles of (a) potential temperature [K], (b) relative humidity [%], with respect to water (ice) above (below) 0°C, and (c) updraught mass flux, averaged over the final 70 days of simulation. Snapshot of surface precipitation rate [mm·hr^{-1}] on day 50 of the simulations from (d) 200 m CRM (native resolution), (e) CTRL and (f) CoMorph-A, both 10 km resolution, (g) time series of f_{sub}, calculated as in the text, for the CRM, CTRL and CoMorph-A. The dashed lines are the CTRL and CoMorph-A results over the large 6000 × 400 km^2 domain. The vertical grey dotted line in (g) shows the timing of the snapshots in (d–f).

This section has shown the mean profiles under RCE and how convection self-aggregates using CoMorph-A, with similar performance to CTRL. The following section will examine how convection is related to mid-tropospheric humidity, and the organisation of convection in the different simulations will be revisited.

3.2 | Sensitivity to tropospheric humidity

For models to adequately represent convective clouds, they must capture the interaction between convection and mid-tropospheric humidity. This moisture–convection

relationship has been found to be important for simulating the MJO (e.g. Hirons et al., 2013; Kim et al., 2014), but is poorly simulated in the UM, in terms of amplitude and propagation across the maritime continent (Williams et al., 2017; Ahn et al., 2020).

The experimental set-up has been kept as similar to Derbyshire et al. (2004) as possible, although accounting for a higher model top in more recent versions of the model. The model is initialised and above 1 km is relaxed back to fixed profiles of potential temperature, zonal wind and relative humidity (RH) with a relaxation time-scale of 1 hr. Between 2 and 16 km there are four different experiments with reference values of RH of 25%, 50%, 70% and 90%. The simulation is run for 5 days with the initial day

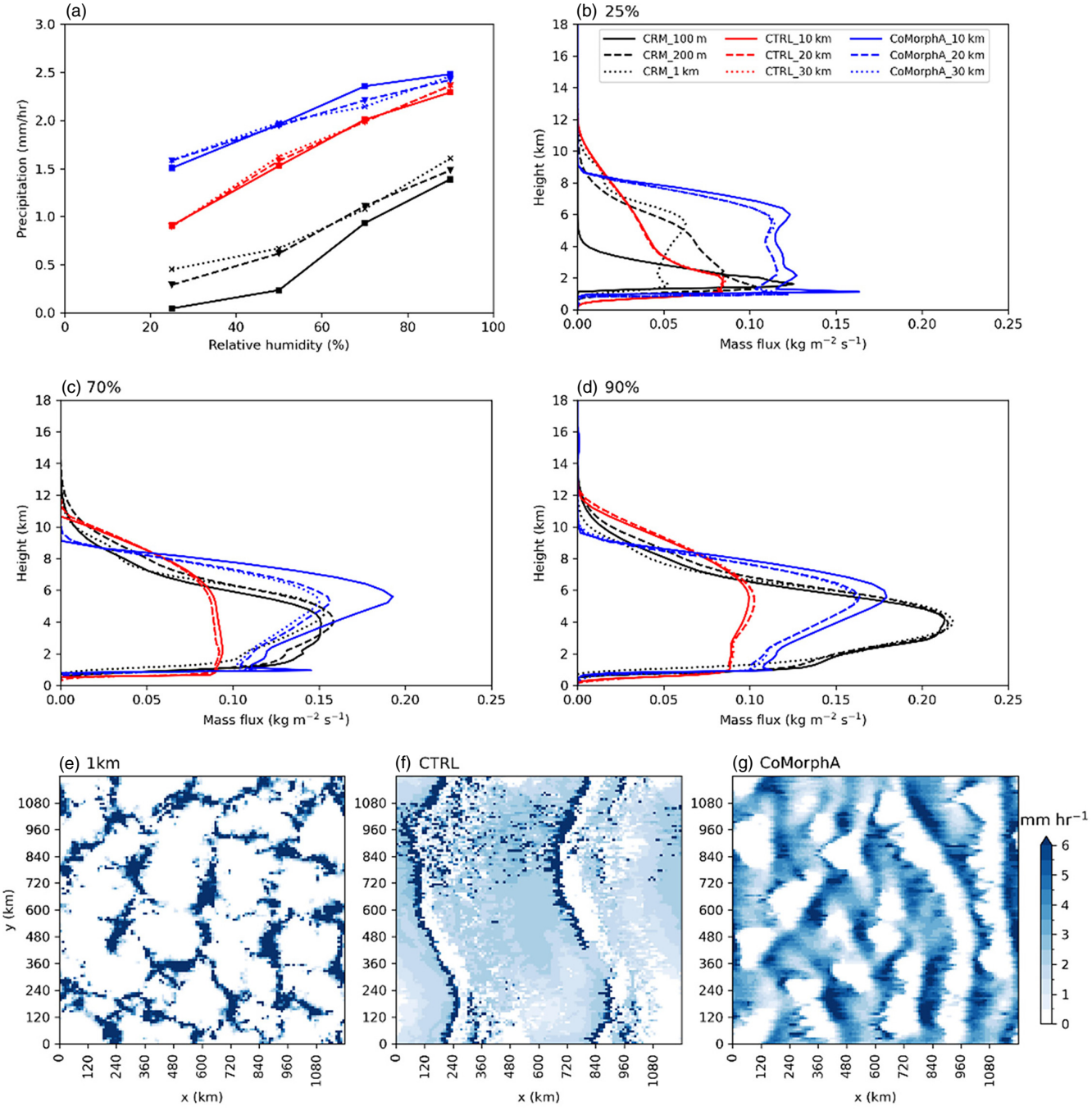

FIGURE 2 EUROCS. (a) Precipitation [mm·hr^{-1}] against relative humidity and (b–d) updraught mass flux [kg·m^{-2}·s^{-1}] for the 25%, 70% and 90% cases. Results for multiple resolutions from the 50 × 50 km^2 domain CRM (black), large (1200 km domain) CTRL (red) and CoMorph-A (blue). Snapshot of surface precipitation rate [mm·hr^{-1}] on day 4 of the 90% case, 1200 × 1200 km^2 domain simulations from the (e) 1 km CRM; re-gridded to same 10 km grid (f) CTRL and (g) CoMorph-A.

discarded from the analysis. The 3D idealised set-up of this case has been useful for investigating propagating convective bands that have been seen in earlier versions of the UM (e.g. Roberts, 2001; Tomassini et al., 2017). In addition to the results shown here for $50 \times 50\,km^2$ (CRM) and $1200 \times 1200\,km^2$ domains, the CRM has been run at 100 m, 200 m, 500 m and 1 km resolution over 25×25, 50×50, and $100 \times 100\,km^2$ domains and CTRL and CoMorph-A at 10, 20, 30 and 60 km resolutions over $100 \times 100\,km^2$ (10 km resolution only), $600 \times 600\,km^2$ and $1200 \times 1200\,km^2$ domain sizes.

The original paper showed the sensitivity to humidity was highly variable depending on the single-column model analysed. While the CRM results show a similar overall increase in precipitation rate from 25% to 90% humidity as documented in Derbyshire et al. (2004), there is clear variation with resolution: The highest resolution (100 m; solid line) tends to have the lowest precipitation values whilst the coarsest resolution (1 km; dotted line) has the largest values, with large differences in the mass-flux profiles for the 25% experiment (Figure 2b), consistent with the results of the original study (fig. 4 in Derbyshire et al., 2004).

Using this experimental set-up, CoMorph-A rapidly responds to the unstable profile and has too high precipitation amounts for all humidity cases (Figure 2a). This is a similar result to the SCMs examined in the original study (see fig. 15 in Derbyshire et al., 2004). The moisture sensitivity is lower in CoMorph-A than CTRL with an increase of $1.0\,mm{\cdot}hr^{-1}$ between the 25% and 90% cases compared to $1.4\,mm{\cdot}hr^{-1}$ in CTRL. CoMorph-A shows more resolution sensitivity than CTRL particularly at the higher humidities but is relatively insensitive to domain size (not shown). The updraught mass-flux profiles from the 70% and 90% experiments (Figure 2c,d) show both parametrized runs peaking at too high altitude relative to the CRM, with CoMorph-A also terminating too low. The peak values of mass flux are more similar to the CRM in CoMorph-A than CTRL, but this is associated with much higher precipitation rates in CoMorph-A. The CRM has additionally been run over the same $1200 \times 1200\,km^2$ domain as CTRL and CoMorph-A but at 1 km resolution. A snapshot of precipitation rate over this large domain after 4 days is shown in Figure 2e–g with the CRM re-gridded to the same 10 km grid as CTRL and CoMorph-A. Both parametrized runs have too much background precipitation and a less cellular structure than is evident in the CRM although this is arguably improved in CoMorph-A relative to CTRL. Developments to allow a greater sensitivity to relative humidity in future versions of CoMorph will be discussed in Section 4.

This is a highly idealised case which relaxes back to the same profiles and, like the RCE, generates a steady state enabling the analysis of mean profiles and precipitation rates as well as the emergent spatial structures. In the following section the model uses time-varying forcings to represent the initiation and development of convection during the day.

3.3 | Diurnal cycle

The failure of models with parametrized convection to fully represent the diurnal cycle is well known, with convection often occurring too early in the day, particularly over land (e.g. Yang & Slingo, 2001). This has been an issue in earlier versions of the UM (e.g. Christopoulos & Schneider, 2021). Here we examine the performance of CoMorph-A at simulating the diurnal cycle using three well-documented experiments examining different aspects of the development of convection: a shallow convection case, transition to deep convection in a semi-arid environment and a midlatitude, deep convection case. All three cases have interactive radiation turned off. To help understand the sensitivity of the parametrized simulations in the single-day cases (ARM and AMMA), an ensemble of six simulations is performed by perturbing the initial random noise.

3.3.1 | Shallow ARM case

The first diurnal case is based on observations made at the midlatitude Southern Great Plains (SGP) site of the Atmospheric Radiation Measurement (ARM) Program on 21 June 1997 (Brown et al., 2002; Lenderink et al., 2004), commonly referred to as the ARM case. This tests the development of shallow cumulus over land with no development to deep convection. The original paper had a very small ($6.4 \times 6.4\,km^2$) domain with a low model top depth (4.4 km) and 40 m vertical resolution. Here, the same operational global and regional stretched grid vertical levels (Bush et al., 2023) are used with a 40 km model top, and consequently the vertical resolution above the near-surface layer is lower.

Figure 3a–c show the evolution of the cloud in the three simulations. In the high-resolution run this is similar to previous studies (fig. 2b in Lenderink et al., 2004; fig. 5 in Brown et al., 2002; fig. 2a in McIntyre et al., 2022). Both CTRL and CoMorph-A overestimate the cloud fraction relative to the high resolution, consistent with early SCM results (Lenderink et al., 2004). The cloud fraction near cloud base is significantly higher in CoMorph-A than both the CRM and CTRL. The evolution of the height of cloud base is well simulated by both parametrized runs and both remain shallow although the cloud-top height

differs between the runs, with CoMorph-A increasing more gradually than CTRL. All runs generate precipitation (Figure 3d) unlike the original simulations where microphysical parametrizations were switched off. CTRL has a small cloud fraction at 1900 UTC, after precipitating, before increasing again in both amplitude and altitude. Both parametrized runs also have a rapid reduction in cloud-top height at the end of the simulation once they stop precipitating. Although the cloud fractions have larger maxima in CTRL and CoMorph-A, the values of updraught mass flux remain lower than the CRM (Figure 3e) and remain almost identical for the different ensemble members.

3.3.2 | AMMA case

The second diurnal case is based on observations from the African Monsoon Multidisciplinary Analysis (AMMA) showing the development of daytime convection in a semi-arid region with a much larger amplitude diurnal cycle (Couvreux et al., 2012). Comparison of Figure 4a with fig. 2 in Couvreux et al. (2015) shows that the CRM differs somewhat from the original LES results, with the onset of precipitation and its subsequent peak occurring ~2 hr earlier. CTRL initiates precipitation almost 2 hr too early relative to the CRM and only persists for 3 hr before abruptly stopping. CoMorph-A initiates an hour earlier than the CRM and has almost double the precipitation rate, which is maintained into the evening.

Observations from the AMMA case-study (fig. 3 in Couvreux et al., 2012) showed the boundary layer grows throughout the morning, reaching 2.5 km in the mid-afternoon, consistent with the present CRM results (Figure 4b). This was associated with a decrease in convective inhibition (CIN; Figure 4c) during the morning. The CRM shows a decrease in boundary-layer height and slight increase in CIN into the evening. Both CTRL and CoMorph-A capture the growth of boundary-layer height and evolution of CIN although these evolve too quickly,

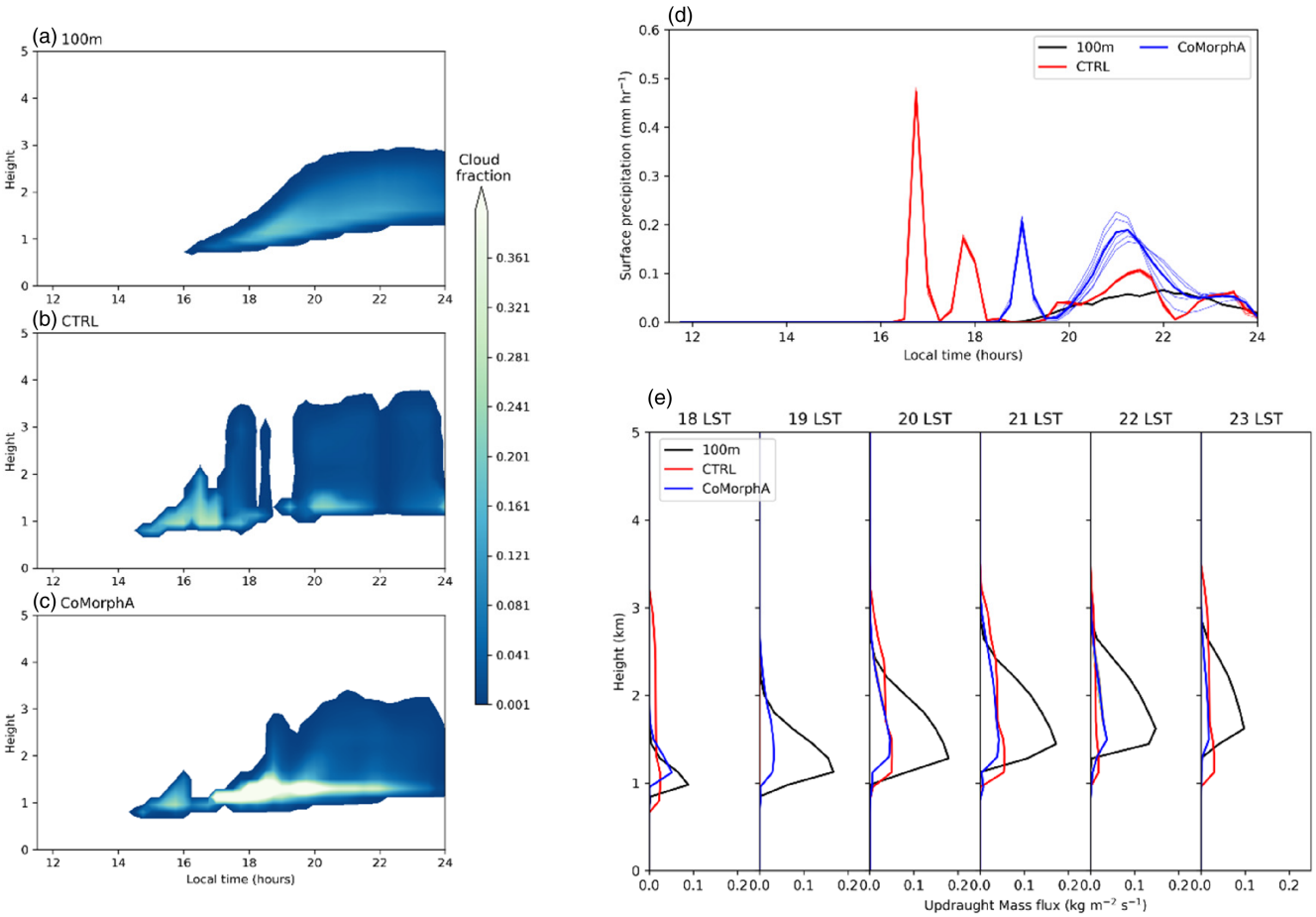

FIGURE 3 Atmospheric radiation measurement (ARM). Time evolution of cloud fraction in (a) 100 m CRM, (b) CTRL and (c) CoMorph-A simulations of the shallow ARM case. (d) Time series of precipitation [mm·hr^{-1}] from the three simulations. (e) Updraught mass flux [kg·m^{-2}·s^{-1}] profiles between 1800 and 2300 local time. (d) and (e) are shown for each ensemble member (thin lines) and the ensemble mean (thick line).

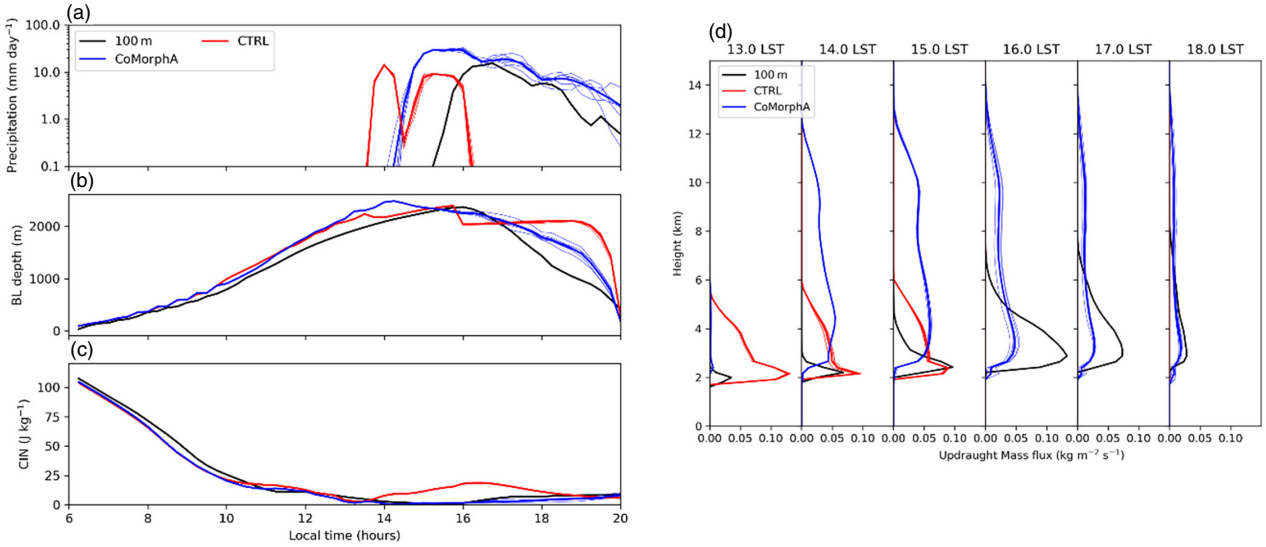

FIGURE 4 African monsoon multidisciplinary analysis (AMMA). Time series of (a) surface precipitation [mm·day^{-1}], (b) boundary-layer depth [m] and (c) CIN [J·kg^{-1}] from the 100 m CRM (black), CTRL (red) and CoMorph-A (blue) ensemble members (thin lines) and ensemble mean (thick line) simulations of the AMMA case. (d) Hourly mass-flux [kg·m^{-2}·s^{-1}] profiles from 1300 to 1800 local time.

consistent with the earlier development of precipitation. The positive values of mass flux (Figure 4d) are confined to lower altitudes in the CRM than CoMorph-A. The CTRL convective mass flux is zero for 1600 LST with only large-scale precipitation contributing to the total surface precipitation rate.

3.3.3 | Deep ARM case

The final diurnal case is based on the same field campaign as in Section 3.3.1 but for a different day (27 June 1997: Guichard et al., 2004) using the experimental set-up of Daleu et al. (2020). The model is forced with surface sensible and latent heat fluxes which vary sinusoidally throughout the day (0–12 hours), reaching a peak at 6 hours and set to zero overnight (12–24 hours) with a prescribed radiative cooling applied to the potential temperature (Daleu et al., 2020). The original papers (Chaboureau et al., 2004; Guichard et al., 2004) applied the same fluxes but with an earlier start time of 6 hours which is accounted for when comparing the results. This forcing is repeated over 10 days to get the mean diurnal cycle, with the initial day excluded from the diurnal means.

The time series of precipitation is shown along with the mean diurnal cycle (Figure 5a,b). All simulations reach peak precipitation rate prior to the peak in surface fluxes (6 hours into run); 3–4 hours earlier than in the original papers (fig. 2a, Chaboureau et al., 2004; fig. 3, Guichard et al., 2004). As with the previous cases, CTRL initiates convection earlier than CoMorph-A and the CRM which is also evident in the updraught mass-flux profiles (Figure 5c). CoMorph-A initiates slightly earlier than the CRM and the peak precipitation rate in both parametrized runs is greater than in the high-resolution run. CTRL peaks at hour 3, decreases until hour 5 before peaking again at hour 8. CoMorph-A precipitation rate reaches an initial peak after 4 hours and then declines rapidly over the next 3 hours before decreasing more gradually until 12 hours. The CRM has a higher rate than CoMorph-A between hours 6 and 9, consistent with the higher values of mass flux at these times. but after this the rate remains similar to CoMorph-A.

This section has highlighted an improvement in the timing of the diurnal cycle using CoMorph-A. The following section extends this diurnal cycle analysis by examining how the development of convection is influenced by previous convection.

3.4 | Memory in the diurnal cycle

Using the set-up from Section 3.3.3 (Guichard et al., 2004), Daleu et al. (2020) introduced a memory function which could be separated into three phases: the first representing the persistence of convection, the second representing the suppression of convection in areas which had precipitation in the previous few hours, and the third representing a secondary enhancement of precipitation. This is calculated for each of the final 9 days of the simulation

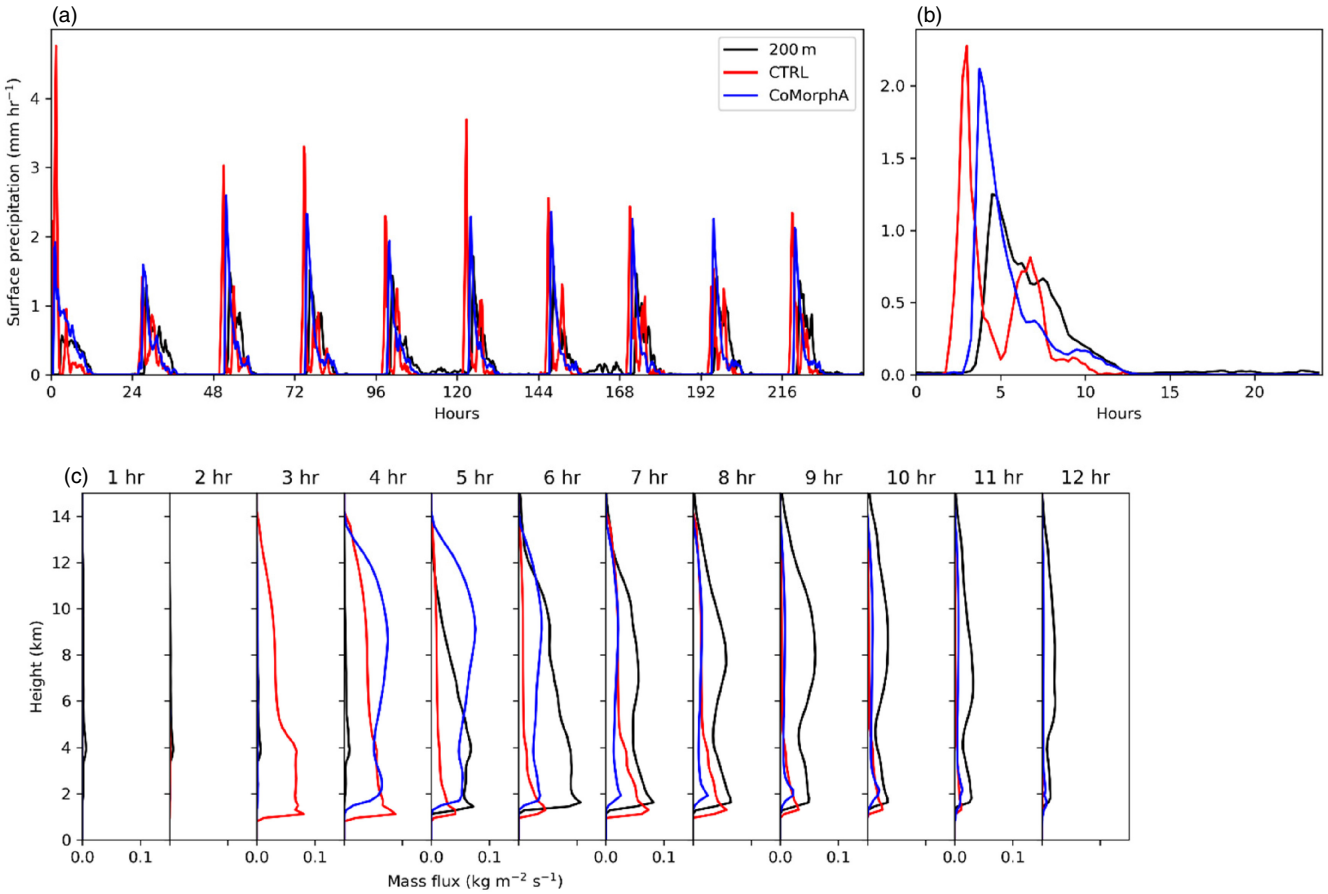

FIGURE 5 Deep atmospheric radiation measurement (ARM). (a) Time series of precipitation [mm·hr^{-1}] over 10 days of the simulation of the deep ARM case, (b) mean diurnal cycle of precipitation [mm·hr^{-1}] and (c) mean updraught mass flux [kg·m^{-2}·s^{-1}] profiles shown for the first 12 hr. Means are calculated over the final 9 days of the simulation.

as with the mean diurnal precipitation rate shown in Figure 5b.

The memory function, M, is defined in Daleu et al. (2020), and is based on the probability of finding rain (mean precipitation greater than 0.1 mm·hr^{-1}) at both time, t_0, and at an earlier time, $t_0 - \Delta t$, over a given area, A, compared to the expected probability assuming that these two events occur independently of each other $\left(P^2[R(A,t_0,\Delta t)] = P[R(A,t_0)] \times P[R(A,t_0-\Delta t)]\right)$:

$$\mathrm{M}(A,t_0,\Delta t) = P[R(A,t_0) \cap R(A,t_0-\Delta t)] - P^2[R(A,t_0,\Delta t)]. \quad (1)$$

A value of zero indicates that there is no memory in the system, while positive values indicate an increased chance of raining at the later time, t_0 if it rained at the earlier time, $t_0 - \Delta t$, and a negative value suggests that there is suppression of rainfall linked to the earlier rainfall event. The threshold for Figure 6 shows the probability of finding rain ($P[R(A,t_0)]$) and the memory function for a box of size $A = 10 \times 10$ km^2 and t_0= 2, 2.5, 3.5, 4, 5, 6, 7, and 8.5 hr after the initial precipitation (triggering). The memory function is set to zero beyond time lags (i.e. prior to triggering).

The results using the UM CRM differ slightly from those in Daleu et al. (2020) which used the Met Office NERC cloud model (MONC: Brown et al., 2015). The results using $A = 4 \times 4$ km^2 are shown for comparison with Figure 6 in the original paper. The UM CRM triggers slightly later than MONC and the increase is more gradual over the initial 30 min, but rainfall remains higher for a longer time. The initial persistence of convection and subsequent suppression (phase 2) is weaker in the CRM than MONC. The secondary enhancement (phase 3) can only be seen after 5 hours for convection produced 8 hours after triggering and is weaker than MONC. The difference between using different values of A ($A = 4 \times 4$ and $A = 10 \times 10$ km^2) are consistent with results using MONC (fig. 5c in Daleu et al., 2020). Results using $A = 10 \times 10$ km^2 for CRM, CTRL and CoMorph-A will now be compared to assess the performance of CoMorph-A.

In the previous section we noted that CTRL triggers over an hour earlier than CoMorph-A and the CRM.

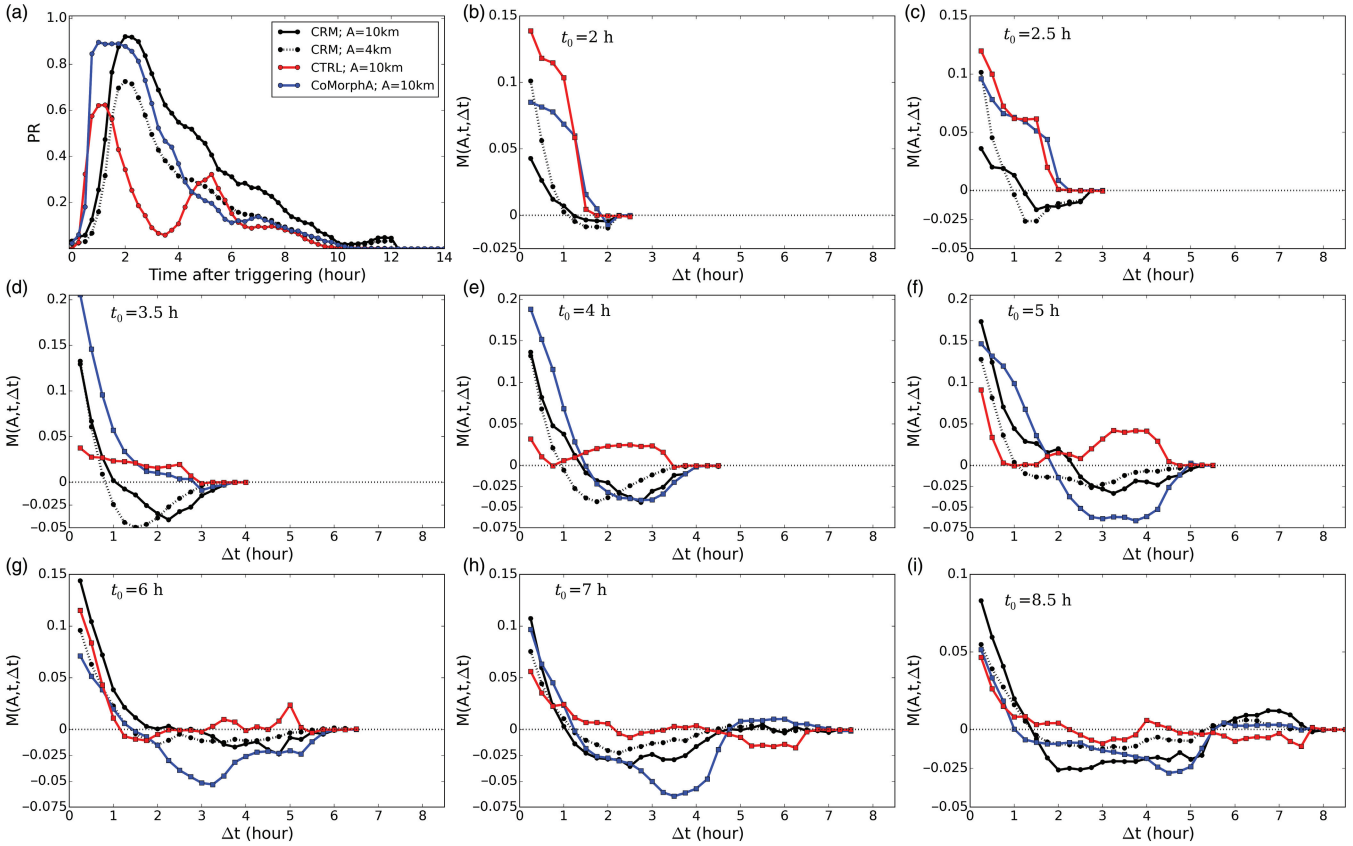

FIGURE 6 Memory case. (a) Probability of finding rain (P[R(A,t_0]) for $A = 10 \times 10$ km^2 in the deep ARM case. The time axis is shifted relative to triggering time such that time 0 corresponds to the time of triggering in all three simulations. Memory function (M[A,t_0,dt]) for $A = 10 \times 10$ km^2 and t_0 = (b) 2, (c) 2.5, (d) 3.5, (e) 4, (f) 5, (g) 6, (h) 7, (i) 8.5 hours after triggering. Results are the ensemble mean obtained in the 200 m CRM (black, solid), CTRL (red) and CoMorph-A (blue) simulations. Results for $A = 4 \times 4$ km^2 are also shown for the CRM (black, dotted).

There are bigger differences in the probability of finding rain (Figure 6a) in the two parametrized simulations than we saw in the rainfall rate in Figure 5 due to differences in the number and spatial size of the events. Both CTRL and CoMorph-A show a higher probability of finding rain over the first hour than the CRM, remaining lower for subsequent times (Figure 6a). The probability of rain in CTRL decreases after the first 2 hr, reaching a minimum 3–4 hr after triggering before increasing again. Neither CoMorph-A or the CRM show this secondary peak. Over the first 2 hours after triggering (first phase), CTRL and CoMorph-A have comparable memory with persistence of convection maintained for longer than the CRM (Figure 6b). The suppression of convection (second phase) in the CRM starts within 1.5 hr for convection produced 2.5 hr after triggering (Figure 6c). For CoMorph, there is an indication of suppression for convection produced before $t_0 = 3.5$ hr (Figure 6d) but this is weak, and only lasts 15 min. For convection produced from $t_0 = 4$ hr (Figure 6e), the initial persistence of convection is followed by a suppression for a further 2.5 hr in both CoMorph-A and CRM with a maximum suppression of 4 hr (for convection produced from $t_0 = 7$ hr; Figure 6h). This suppression of convection happens much later in CTRL and is only evident after 5 hr for convection produced over 7 hr after triggering (Figure 6g–i). The secondary enhancement of convection (third phase) is weak but evident in the CRM for convection produced over 8.5 hr after triggering (Figure 6i). This weak secondary enhancement can also be seen in CoMorph-A for convection produced at $t = 7$ hr (Figure 6h) but is not captured by CTRL. It is found that this secondary enhancement can be enhanced using CoMorph-A but with a fixed low entrainment rate (not shown).

These results show that CoMorph-A has a more realistic relationship between earlier precipitation than CTRL and although it is able to capture the secondary enhancement form of memory, the timings and strength vary from the CRM. This was a multi-day case but applying the same forcing each day to build up an ensemble. The next section evaluates a multi-day case using time-varying forcing based on observations to show the performance

of CoMorph-A in simulating convective systems over a longer time period.

3.5 | Multi-day tropical case

The multi-day analysis uses a well-documented case based on observations from the Tropical Warm Pool–International Cloud Experiment (TWP-ICE: May et al., 2008) using a set-up based on Fridlind et al. (2012). This involves a 16-day period during the Australian monsoon featuring an active monsoon period followed by suppressed conditions and a monsoon break (May et al., 2008). This case has interactive radiation, so provides evaluation of the influence of cloud–radiative feedback on CoMorph but is highly constrained by the nudging to observational data.

The CRM results compare well with other models (Petch et al., 2014). The peak precipitation values differ slightly from observed as they did in the original comparison (Fridlind et al., 2012; Petch et al., 2014), particularly when there is only very light precipitation in the later part of the period. CTRL shows more high-frequency variability than CoMorph-A.

The mass-flux profiles from the wet and dry periods are shown in Figure 7. The mass-flux profiles from the wet period are very similar to those from the 90% EUROCS case (Figure 2d) with the parametrized runs peaking at higher altitude than the CRM. Like that case, CoMorph-A has a higher mass flux than CTRL while both are lower than the CRM peak. Although, in this case both parametrized runs terminate 4 km lower than the CRM, again suggesting a need for the representation of overshoots in the parametrization. For the dry period all mass-flux profiles show the expected bottom-heavy profile and terminate at the same altitude. The CRM has a higher mass flux throughout the profile than both parametrized runs. Compared to CTRL, CoMorph-A has a lower mass flux in the

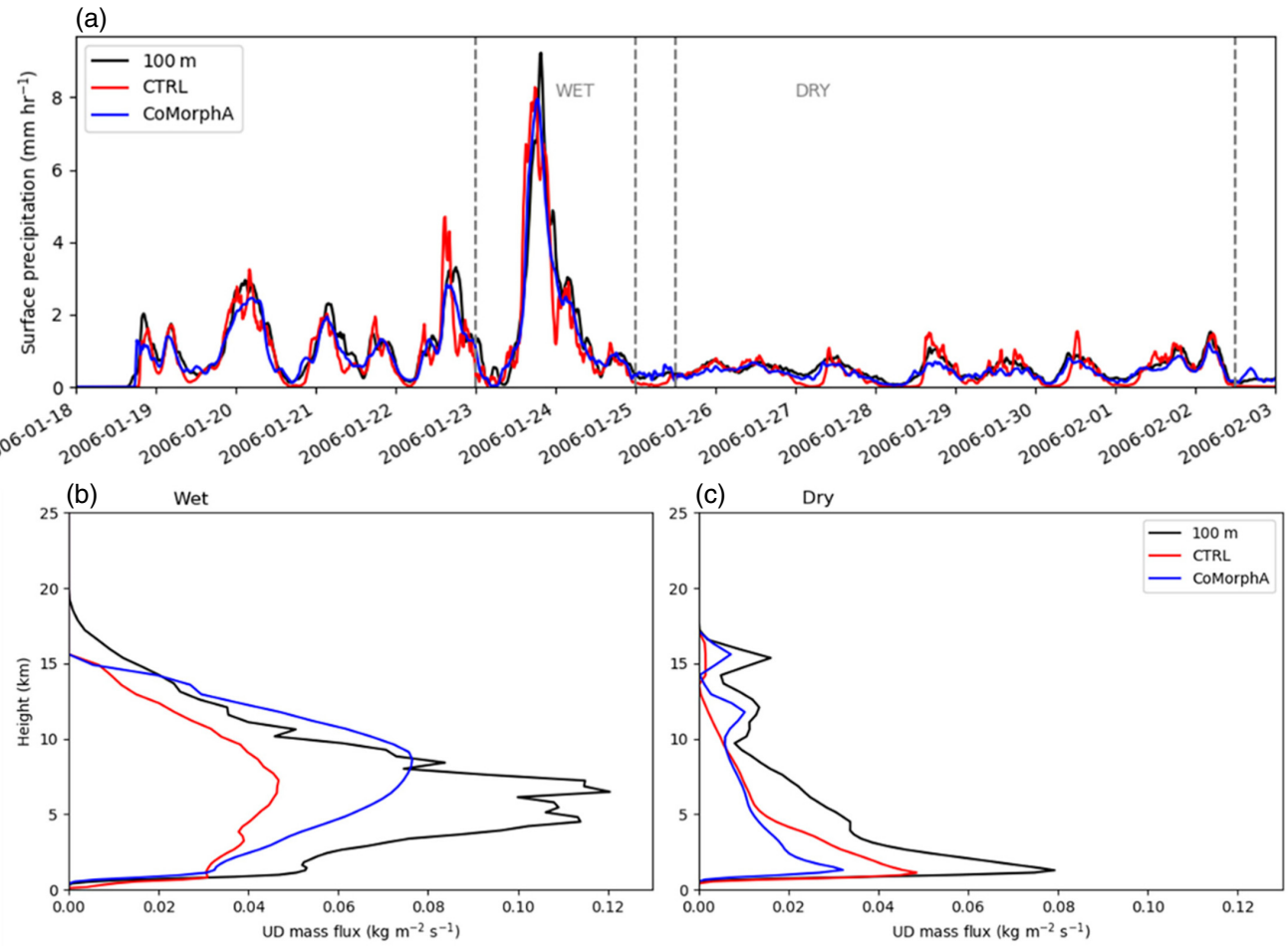

FIGURE 7 Tropical warm pool–international cloud experiment (TWP-ICE). (a) Time series of 15 min precipitation rates [mm·hr^{-1}], and mean updraught mass flux [kg·m^{-2}·s^{-1}] during the (b) wet and (c) dry period of TWP-ICE from the 100 m CRM (black), CTRL (red) and CoMorph-A (blue) simulations. The wet and dry periods are shown by the grey dashed lines on (a).

lower troposphere but higher in the upper troposphere. The CoMorph-A results from the dry period are very different from the 25% humidity case shown in Section 3.2 (Figure 2b) suggesting that under a different experimental set-up CoMorph-A could be more sensitive to humidity than the earlier results implied.

All cases so far have assumed a homogenous surface. The following section details a new idealised case for evaluating the behaviour of convection when there is a strip of land (an island) in the domain and how this affects the propagation of convection under different wind regimes.

3.6 | Inland propagation and nocturnal convection

The Maritime Continent is difficult to represent accurately, with the initiation of convection by the convergence of sea-breeze circulations (Birch et al., 2015) and offshore gravity waves (Love et al., 2011) being vital for simulation of the region. An idealised island case has been developed to analyse this behaviour and examine the ability of propagation of convection both on and off land. This new set-up has an idealised island set at the Equator, with interactive radiation and a real sandy land surface with plenty of

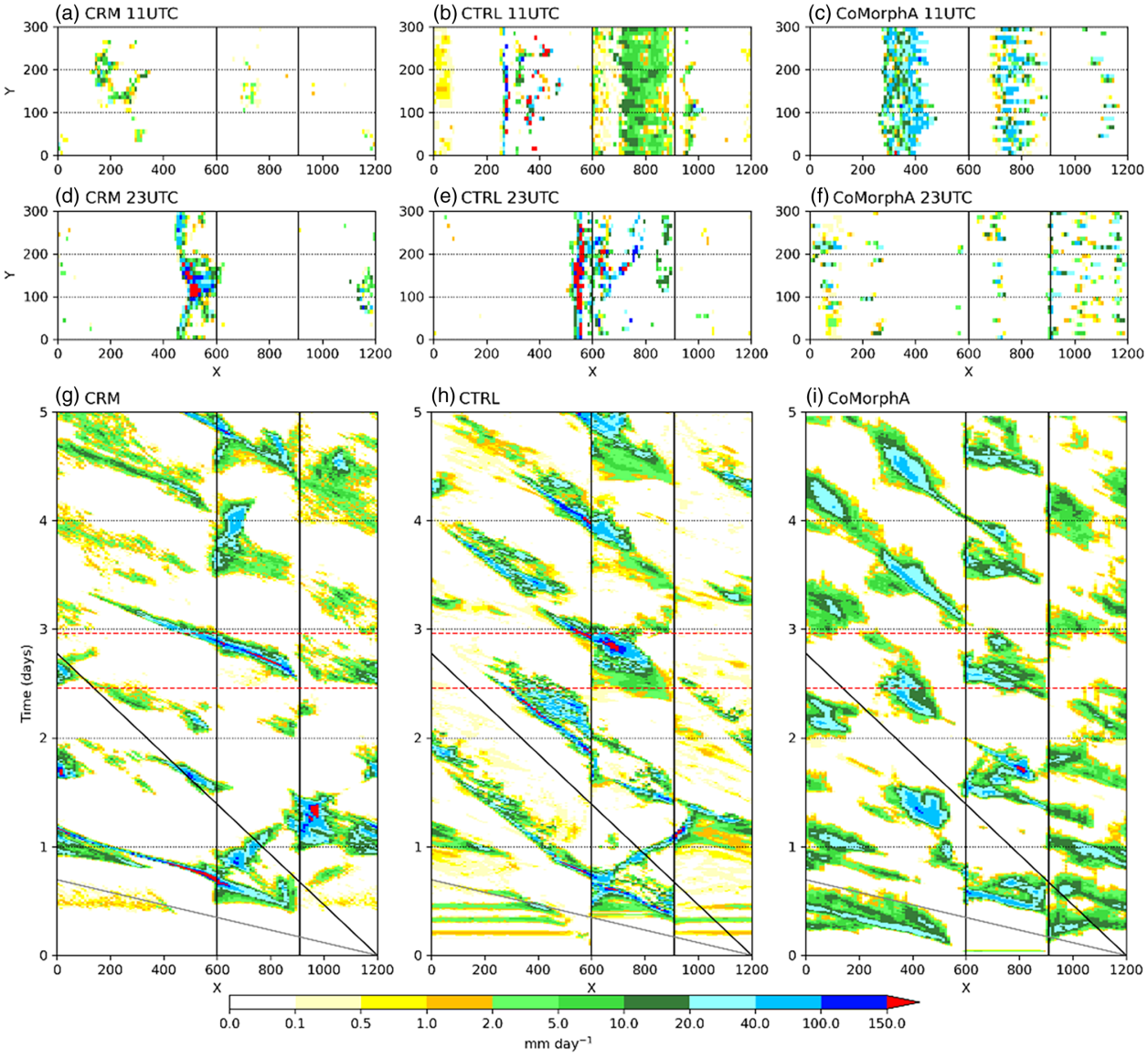

FIGURE 8 Island case. Snapshots of precipitation [mm·day^{-1}] at (a–c) 1100 and (d–f) 2300 UTC on day 3 of the island simulation with a 5 m·s^{-1} background wind ($U = 5$) for (a,d) the CRM; regridded to 10 km, (b,e) CTRL and (c,f) CoMorph-A. Hovmüller of precipitation [mm·day^{-1}] averaged over full y-domain from (g) CRM (250 m; re-gridded to 10 km), (h) CTRL and (i) CoMorph-A. The vertical black lines show the location of land ($x = 600$–900 km). The diagonal black line shows the background wind (5 m·s^{-1}) with the grey line showing 20 m·s^{-1}. Red dashed lines show the times of the snapshots in (a–f).

moisture initially. It has been run with ($U = 5\,\mathrm{m{\cdot}s^{-1}}$; Figure 8) and without a background wind ($U = 0\,\mathrm{m{\cdot}s^{-1}}$; Figure 9). The case with the wind has a gravity wave propagating off the land initiating convection over the sea due to the heating profile of late afternoon convection over the land. The case with no wind illustrates the impact of land/sea breezes.

With a background wind (Figure 8), snapshots of precipitation rate at 11am and 11pm show the location of precipitation in each simulation. At 11am on day 3 there is much more rain over land in the parametrized runs than the high-resolution CRM (Figure 8a–c), although there is a line of precipitation over the ocean in all three simulations. At 11pm (Figure 8d–f) there is a distinct line of precipitation associated with the gravity wave in the CRM. The CTRL has convection just off-land which is not evident in CoMorph-A.

Propagation in the CRM (Figure 8g) is much quicker ($\sim 20\,\mathrm{m{\cdot}s^{-1}}$) than the lower-resolution parametrized convection runs (Figure 8h,i) which propagate at a similar speed to the background wind ($5\,\mathrm{m{\cdot}s^{-1}}$), particularly over the ocean. CoMorph-A propagates at this higher speed over land but struggles to propagate off the land, unlike CTRL which is better at capturing this. CoMorph-A has widespread mid-intensity precipitation but not the very high intensities shown in CTRL.

The case with no background wind (Figure 9a) shows precipitation over the island tending to start close to the coasts, likely initiated by sea breezes, and gradually moving inland. Later in the day the convection tends to become more widespread over the land. On some days convection propagates for a small distance off land which is possible evidence of cold pools and land/sea breezes. Both CTRL and CoMorph-A (Figure 9b,c) show no evidence of the convection over land starting at the coasts; instead there is some evidence of convection in the centre of the island starting far too early. This island set-up shows some more work is needed to correctly represent the interaction with sea breezes in CoMorph-A and will be a useful testbed during future development of the scheme.

In the final case, we show the impact of different tunings on the representation of CMT and the utility of idealised cases to inform tunings of the GCM.

3.7 | Convective momentum transport

The transport of momentum vertically by convection (i.e. CMT) is an important process, significantly affecting upper-level wind speeds in global models (e.g. Gregory et al., 1997), and needs to be parametrized. The cold air outbreak case from Kershaw & Gregory (1997) is

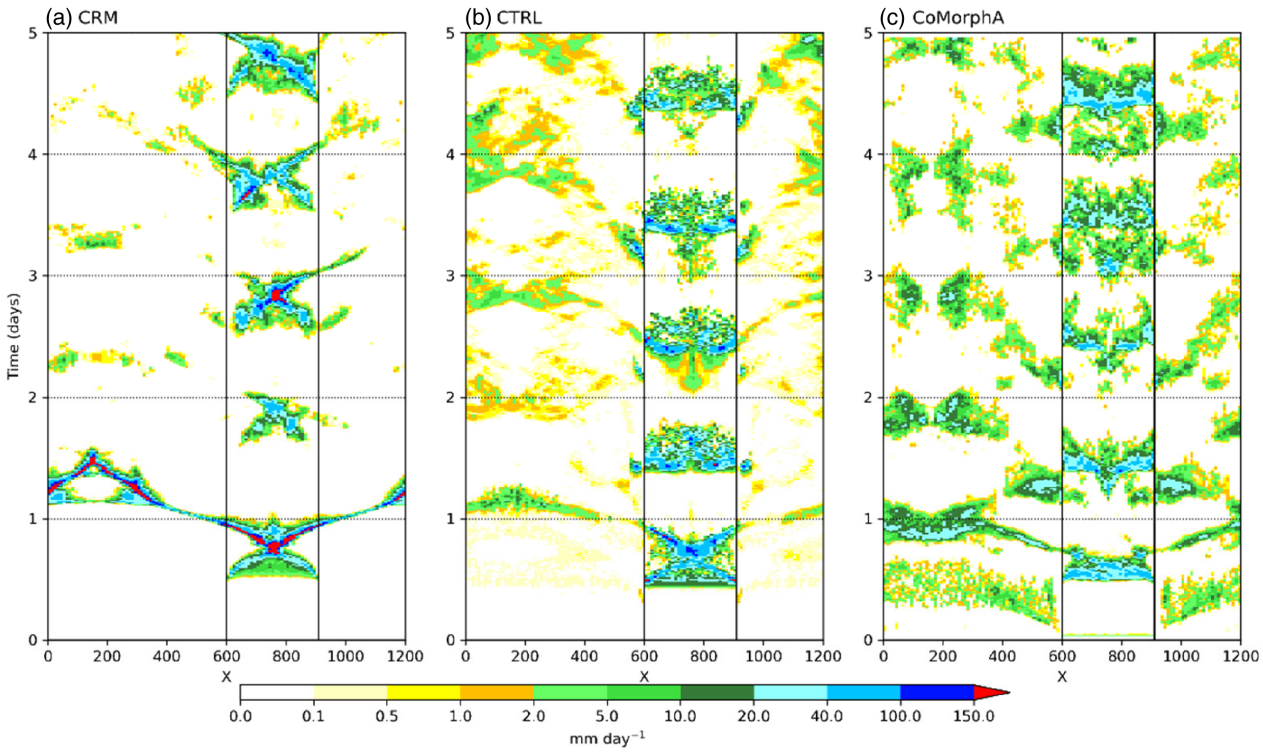

FIGURE 9 Island case. Hovmüller (averaged over full y-domain) of precipitation [$\mathrm{mm{\cdot}day^{-1}}$] from (a) CRM (250 m; regridded to 10 km), (b) CTRL and (c) CoMorph-A from simulations of the idealised island with no background wind ($U = 0$).

used to test CoMorph's CMT behaviour. The CRM profiles (black dotted, Figure 10) are similar to the results documented in the original paper (figs 7 and 9 in Kershaw & Gregory, 1997). The mass-flux profiles (Figure 10a,b,e,f) differ between the parametrized and CRM results with CoMorph-A having a secondary peak in updraught mass flux at 5–6 km altitude compared with CTRL and CRM where there is a single peak just above cloud base (Figure 10a,e). The CTRL downdraught mass flux remains fairly uniform with height whereas both CoMorph-A and CRM show a peak at 1 km. Since the mass-flux profiles are different between the simulations, we do not expect to have the same wind profile; however, by changing the CMT calculation we can see the effect on these profiles. The shallower updraught mass-flux profile in the CRM than the parametrized runs results in the winds reaching the maximum value at lower altitude. Without the inclusion of CMT the resulting winds are too weak at low levels and too strong above 2 km (grey solid line; Figure 10c,g). Originally the CMT was applied without a pressure gradient term to account for the difference between in-cloud and environmental momentum, resulting in the overly strong damping of the upper-level winds (grey dotted line; Figure 10c,g) which was also evident in global simulations (not shown). Adding in a pressure gradient term with a quadratic drag law leads to damping of the winds to an appropriate level, taking into consideration that the mass-flux profile does not compare perfectly with the CRM. The sensitivity to the value of the drag coefficient in the pressure gradient term is also shown with a lower drag (dashed lines)

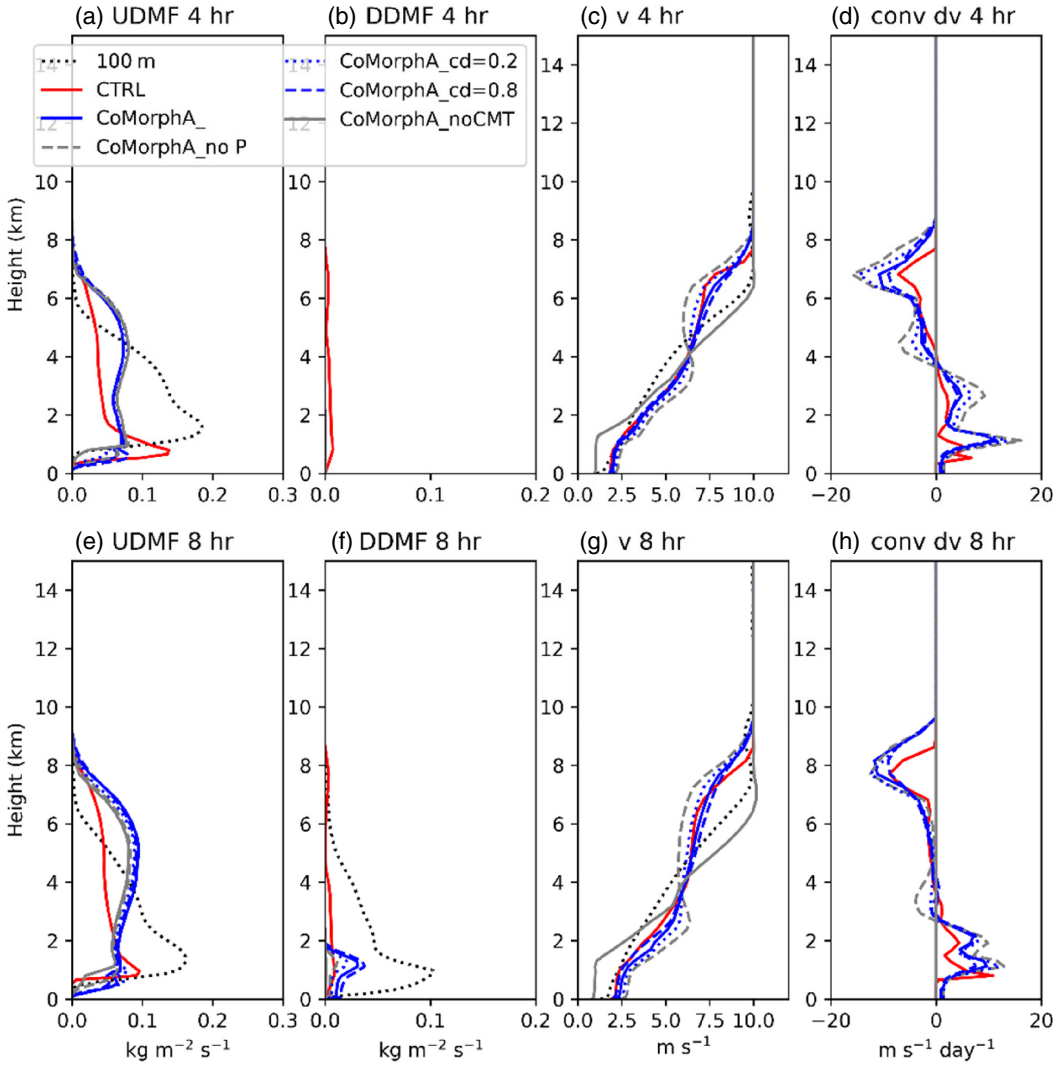

FIGURE 10 Convective momentum transport (CMT). Profiles at 4 hr of (a) updraught mass flux [kg·m^{-2}·s^{-1}], (b) downdraught mass flux [kg·m^{-2}·s^{-1}], (c) meridional wind [m·s^{-1}] and (d) the increment in meridional wind due to convection [m·s^{-1}·day^{-1}] in the parametrized runs for the cold air outbreak case. (e–h) As (a–d) but 8 hr into the run. Results shown for the 100 m CRM (black), CTRL (red) and various configurations of CoMorph: CoMorph-A (blue, solid), CoMorph-A with no CMT (grey), CoMorph-A but no pressure term in the CMT calculation (grey, dashed), drag coefficient of 0.2 (blue, dotted) and 0.8 (blue, dashed).

resulting in convection being more efficient at transporting momentum in the vertical (e.g. Figure 8c,d,g,h). The magnitudes of the convective increment to meridional winds are similar between CTRL and CoMorph-A.

This final case has shown the impact of different formulations and tunings of the parametrization on the results. The following section will bring all these cases together and summarise the results.

4 | SUMMARY AND CONCLUSIONS

CoMorph is a new convection scheme developed for the UM, a model which is used extensively across the globe by various institutions. The CoMorph-A package has been shown to perform well in a global configuration, with a reduction of biases under climate configuration and improved NWP performance (A. Lock, submitted work). Although ultimately it is the GCM performance that determines if a scheme becomes operational, throughout development the scheme has been tested using a 3D idealised UM which uses the same science configuration as the full GCM but is substantially cheaper to run. This has allowed us to understand in detail how the model behaves as a function of regime. The present study has documented the performance of CoMorph-A in a selection of idealised experiments, ranging from highly idealised with only high-resolution convection-resolving data as a reference to those based on observational field campaigns with real data and previous intercomparison studies to compare against. Although a number of these cases were initially designed for SCM comparisons, the use of the 3D idealised model has several advantages: evaluation at higher resolutions with the same physics, dynamics and coupling as used in the full GCM, comparison of the emergent organisation and spatial structures, and allowing interaction with the winds leading to propagation of convection (Section 3.6). The results are designed to serve as a baseline for others to compare against, and for assessing performance as CoMorph evolves over the coming years.

CoMorph-A showed some organisation of convection when in RCE, consistent with the majority of models compared in RCEMIP (Wing et al., 2020). The structures from the sensitivity to humidity case showed the emergence of cellular behaviour that was observed in the high-resolution reference. However, both parametrized runs produce too widespread precipitation throughout the domain compared to the CRM. Profiles of updraught mass flux have shown that the peak value is consistently greater in the high-resolution simulations than the parametrized runs, although with lower associated precipitation rates. This may point to a need for stronger downdraught representation in CoMorph in future. The sharper inversion and low termination of updraught mass flux relative to the CRM also suggest the need for a representation of overshoots.

All three diurnal cycle experiments (Section 3.3) show improvements in the timing of the triggering and peak in precipitation over CTRL but still trigger too early relative to high-resolution simulations. This is consistent with the results from global simulations (A. Lock, submitted work) where, although some regions such as parts of Africa have a degradation in the diurnal cycle compared to the control, other regions are improved but still precipitate too early in the day. The peak precipitation is too high across the three cases, with the mass flux showing convection is too deep in most cases. Use of the memory function (Section 3.4) shows CoMorph-A has a more realistic response to earlier precipitation than CTRL. A number of cases (Figures 4, 5 and 10) show CoMorph has a more top-heavy mass-flux profile than CTRL. This is likely due to convection triggering from multiple different heights in the column as well as differences in the detrainment and entrainment formulation.

Overall, CoMorph-A is shown to perform competitively against the existing science configuration. However, as might be expected with the development of a new convection scheme, there are still areas for improvement. In addition to the timing and amplitude of the diurnal cycle of precipitation mentioned above, difficulties in simulating the propagation of convection off land and representing sea breezes in CoMorph-A are made evident using the idealised island case (Section 3.6). CoMorph-A is shown to have too little sensitivity to humidity using the Derbyshire et al. (2004) experimental set-up (Figure 2) with little variation in the mass-flux profiles. These results suggest the need to suppress convection at lower humidities (e.g. Hirons et al., 2013) and based on this experiment it is perhaps surprising that CoMorph-A shows improvements in the representation of the MJO (A. Lock, submitted work). However, the mass-flux profiles do vary greatly between the wet and dry periods of the TWP-ICE experiment (Figure 7) suggesting this sensitivity may be increased under a different experimental set-up. Using an SCM, Daleu et al. (2023) found the relationship between precipitation and column relative humidity was well represented by CoMorph-A in dry environments but breaks down above 70% relative humidity. This sensitivity and the difference in results depending on the experiment need to be investigated further using additional tests.

Many of the convective-scale processes parametrized in CoMorph carry significant uncertainties. In recognition of this, many of the formulae within the scheme are scaled by dimensionless "tuning factors" which can be easily changed. CoMorph has around 30 of these

tuneable parameters, scaling the initial parcel perturbations, entrainment (and its sensitivity to convective organisation), detrainment, various in-plume microphysical processes, the area-fractions of convective cloud and precipitation passed to other parts of the model, and other processes. In CoMorph A, many of these parameters have been tuned over successive versions to ensure both model-stability and good global performance. Section 3.7 illustrates the need for a convection scheme to consider the sub-grid transport of momentum by convection without which the upper-level winds are too strong. How the CMT is parametrized, and the sensitivity to the drag coefficient, required careful consideration to perform well in both global and idealised simulations. This is the only section where the sensitivity of the results to parameters within CoMorph has been discussed. However, it is worth noting that the CoMorph-A entrainment rate is variable depending on the previous time-step precipitation rate, a development that was included based on global testing and is found to improve the performance in climate simulations. Many of the idealised cases have additionally been run with a fixed (high or low) entrainment rate. The higher entrainment rate is found to be beneficial for some cases such as increasing the sensitivity to humidity and the timing of triggering of precipitation in the diurnal cycle experiments, but the lower entrainment is necessary for TWP-ICE and capturing the secondary enhancement of convection in the convective memory (not shown). Global analysis suggests the tropical mean temperature profiles are particularly sensitive to the parameters controlling entrainment, detrainment and in-plume ice processes. Subtropical light rain (which exerts a strong influence on climate sensitivity) is very sensitive to the in-parcel cloud-to-rain autoconversion and precipitation fraction parameters. A more detailed analysis of the sensitivity to a range of parameters may form the basis of future work.

There are several proposed improvements to CoMorph to help address the discussed deficiencies. These include the representation of a second updraught type such that both surface-driven and cold-pool forced convection are represented and allow the proportion of cold-pool forced updraughts to grow more gradually as more deep clouds are initiated. This, along with various additional scientific improvements, including the representation of overshoots and formulation of downdraughts highlighted in this study, will be included in a future release of CoMorph. At the time of writing, the next release of CoMorph is undergoing extensive testing over a range of experiments, including the idealised experiments discussed in the current study. Subsequently, the aim is to couple CoMorph with the C-POOL prognostic cold-pool scheme (Rooney et al., 2022) and enhance the scale-aware properties of the scheme for running at higher (<10 km) resolutions.

ACKNOWLEDGMENT

Sally L. Lavender is funded through the Northern Australia Climate Program (NACP), funded by Meat and Livestock Australia, the Queensland Government through the Drought and Climate Adaptation Program, and the University of Southern Queensland. CD, RP and J-FG gratefully acknowledge funding from NERC grant NE/N013743/1 as part of the ParaCon programme (https://www.metoffice.gov.uk/research/approach/collaboration/paracon). The authors thank two anonymous reviewers for their detailed and insightful comments that helped to improve the manuscript. Open access publishing facilitated by University of Southern Queensland, as part of the Wiley - University of Southern Queensland agreement via the Council of Australian University Librarians.

DATA AVAILABILITY STATEMENT

The data generated from the model simulations used in this paper can be made available by the lead author and Met Office co-authors.

ORCID

Sally L. Lavender https://orcid.org/0000-0003-4785-1569
Alison J. Stirling https://orcid.org/0000-0002-2566-3316
Michael Whitall https://orcid.org/0009-0005-8465-0573
Rachel A. Stratton https://orcid.org/0000-0001-5795-6247
Chimene L. Daleu https://orcid.org/0000-0003-2075-4902
Robert S. Plant https://orcid.org/0000-0001-8808-0022
Adrian Lock https://orcid.org/0000-0001-6289-030X
Jian-Feng Gu https://orcid.org/0000-0002-7752-4553

REFERENCES

Ahn, M.-S., Kim, D., Kang, D., Lee, J., Sperber, K.R., Gleckler, P.J. et al. (2020) MJO propagation across the maritime continent: are CMIP6 models better than CMIP5 models? *Geophysical Research Letters*, 47, e2020GL087250. Available from: https://doi.org/10.1029/2020GL087250

Arakawa, A. & Schubert, W.H. (1974) Interaction of a cumulus cloud ensemble with the large-scale environment, part I. *Journal of the Atmospheric Sciences*, 31(3), 674–701.

Birch, C.E., Roberts, M.J., Garcia-Carreras, L., Ackerley, D., Reeder, M.J., Lock, A.P. et al. (2015) Seabreeze dynamics and convection initiation: the influence of convective parameterization in weather and climate model biases. *Journal of Climate*, 28(20), 8093–8108. Available from: https://doi.org/10.1175/JCLI-D-14-00850.1

Brown, A., Milton, S., Cullen, M., Golding, B., Mitchell, J. & Shelly, A. (2012) Unified modeling and prediction of weather and climate:

a 25 year journey. *Bulletin of the American Meteorological Society*, 93, 1865–1877. Available from: https://doi.org/10.1175/BAMS-D-12-00018.1

Brown, A.R., Cederwall, R.T., Chlond, A., Duynkerke, P.G., Golaz, J.-C., Khairoutdinov, M. et al. (2002) Large-eddy simulation of the diurnal cycle of shallow cumulus convection over land. *Quarterly Journal of the Royal Meteorological Society*, 128, 1075–1093.

Brown, N., Weiland, M., Hill, A., Shipway, B., Maynard, C., Allen, T. et al. (2015) A highly scalable Met Office NERC cloud model. In: *Proceedings of the 3rd international conference on exascale applications and software*. Edinburgh, UK: University of Edinburgh, pp. 132–137.

Bush, M., Boutle, I., Edwards, J., Finnenkoetter, A., Franklin, C., Hanley, K. et al. (2023) The second Met Office Unified Model –JULES regional atmosphere and land configuration, RAL2. *Geoscientific Model Development*, 16, 1713–1734. Available from: https://doi.org/10.5194/gmd-16-1713-2023

Chaboureau, J.-P., Guichard, F., Redelsperger, J.-L. & Lafore, J.-P. (2004) The role of stability and moisture in the diurnal cycle of convection over land. *Quarterly Journal of the Royal Meteorological Society*, 130, 3105–3117. Available from: https://doi.org/10.1256/qj.03.132

Christopoulos, C. & Schneider, T. (2021) Assessing biases and climate implications of the diurnal precipitation cycle in climate models. *Geophysical Research Letters*, 48, e2021GL093017. Available from: https://doi.org/10.1029/2021GL093017

Couvreux, F., Rio, C., Guichard, F., Lothon, M., Canut, G., Bounoil, D. et al. (2012) Initiation of daytime local convection in a semi-arid region analysed with high resolution simulations and AMMA observations. *Quarterly Journal of the Royal Meteorological Society*, 138, 56–71.

Couvreux, F., Roehrig, R., Rio, C., Lefebvre, M.-P., Caian, M., Komori, T. et al. (2015) Representation of daytime moist convection over the semi-arid tropics by parametrizations used in climate and meteorological models. *Quarterly Journal of the Royal Meteorological Society*, 141, 2220–2236. Available from: https://doi.org/10.1002/qj.2517

Daleu, C.L., Plant, R.S., Stirling, A.J. & Whitall, M. (2023) Evaluating the CoMorph-A parametrization using idealized simulations of the two-way coupling between convection and large-scale dynamics. *Quarterly Journal of the Royal Meteorological Society*, 149(757), 3087–3109. Available from: https://doi.org/10.1002/qj.4547

Daleu, C.L., Plant, R.S., Woolnough, S.J., Stirling, A.J. & Harvey, N.J. (2020) Memory properties in cloud-resolving simulations of the diurnal cycle of deep convection. *Journal of Advances in Modeling Earth Systems*, 12, e2019MS001897. Available from: https://doi.org/10.1029/2019MS001897

Derbyshire, S.H., Beau, I., Bechtold, P., Grandpeix, J.-Y., Piriou, J.-M., Redelsperger, J.-L. et al. (2004) Sensitivity of moist convection to environmental humidity. *Quarterly Journal of the Royal Meteorological Society*, 130, 3055–3079. Available from: https://doi.org/10.1256/qj.03.130

Fridlind, A.M., Ackerman, A.S., Chaboureau, J.-P., Fan, J., Grabowski, W.W., Hill, A.A. et al. (2012) A comparison of TWP-ICE observational data with cloud-resolving model results. *Journal of Geophysical Research*, 117(D5), D05204. Available from: https://doi.org/10.1029/2011JD016595

Grabowski, W.W., Bechtold, P., Cheng, A., Forbes, R., Halliwell, C., Khairoutdinov, M. et al. (2006) Daytime convective development over land: A model intercomparison based on LBA observations. *Quarterly Journal of the Royal Meteorological Society,* 132(615), 317–344. Available from: https://doi.org/10.1256/qj.04.147

Gregory, D. & Rowntree, P.R. (1990) A mass-flux convection scheme with representation of cloud ensemble characteristics and stability dependent closure. *Monthly Weather Review*, 118, 1483–1506.

Gregory, D., Kershaw, R. & Inness, P. M. (1997) Parametrization of momentum transport by convection. II: Tests in single-column and general circulation models. *Quarterly Journal of the Royal Meteorological Society*, 123(541), 1153–1183. Available from: https://doi.org/10.1002/qj.49712354103

Guichard, F., Petch, J.C., Redelsperger, J.-L., Bechtold, P., Chaboureau, J.-P., Cheinet, S. et al. (2004) Modelling the diurnal cycle of deep precipitating convection over land with cloud-resolving models and single-column models. *Quarterly Journal of the Royal Meteorological Society*, 130, 3139–3172. Available from: https://doi.org/10.1256/qj.03.145

Hirons, L.C., Inness, P., Vitart, F. & Bechtold, P. (2013) Understanding advances in the simulation of intraseasonal variability in the ECMWF model. Part II: the application of process-based diagnostics. *Quarterly Journal of the Royal Meteorological Society*, 139, 1427–1444. Available from: https://doi.org/10.1002/qj.2059

Hwong, Y.-L., Sherwood, S.C. & Fuchs, D. (2022) Can We Use 1D Models to Predict 3D Model Response to Forcing in an Idealized Framework?. *Journal of Advances in Modeling Earth Systems*, 14(4). Available from: https://doi.org/10.1029/2021ms002785

Kershaw, R. & Gregory, D. (1997) Parametrization of momentum transport by convection. I: theory and cloud modelling results. *Quarterly Journal of the Royal Meteorological Society*, 123, 1133–1151.

Kim, D., Kug, J. & Sobel, A.H. (2014) Propagating versus nonpropagating Madden –Julian oscillation events. *Journal of Climate*, 27, 111–125. Available from: https://doi.org/10.1175/JCLI-D-13-00084.1

Lenderink, G., Siebesma, A.P., Cheinet, S., Irons, S., Jones, C.G., Marquet, P. et al. (2004) The diurnal cycle of shallow cumulus clouds over land: a single-column model intercomparison study. *Quarterly Journal of the Royal Meteorological Society*, 130, 3339–3364. Available from: https://doi.org/10.1256/qj.03.122

Love, B.S., Matthews, A.J. & Lister, G.M.S. (2011) The diurnal cycle of precipitation over the maritime continent in a high-resolution atmospheric model. *Quarterly Journal of the Royal Meteorological Society*, 137, 934–947. Available from: https://doi.org/10.1002/qj.809

May, P.T., Mather, J.H., Vaughan, G. & Jakob, C. (2008) Characterizing oceanic convective cloud systems—the Tropical Warm Pool International Cloud Experiment. *Bulletin of the American Meteorological Society*, 154, 153–155. Available from: https://doi.org/10.1175/BAMS-89-2-153

McIntyre, W.A., Efstathiou, G.A. & Thuburn, J. (2022) A two-fluid single-column model of turbulent shallow convection. Part III: results and parameter sensitivity. *Quarterly Journal of the Royal Meteorological Society*, 148, 3832–3851. Available from: https://doi.org/10.1002/qj.4390

Petch, J., Hill, A., Davies, L., Fridlind, A., Jakob, C., Lin, Y. et al. (2014) Evaluation of intercomparisons of four different types of model simulating TWP-ICE. *Quarterly Journal of the Royal Meteorological Society*, 140, 826–837. Available from: https://doi.org/10.1002/qj.2192

Rio, C., Hourdin, F., Grandpeix, J.-Y., & Lafore, J.-P. (2009) Shifting the diurnal cycle of parameterized deep convection over land. *Geophysical Research Letters*, 36(7). Available from: https://doi.org/10.1029/2008gl036779

Rio, C., Grandpeix, J.-Y., Hourdin, F., Guichard, F., Couvreux, F., Lafore, J.-P. et al. (2013) Control of deep convection by sub-cloud lifting processes: the ALP closure in the LMDZ5B general circulation model. *Climate Dynamics*, 40(9–10), 2271–2292. Available from: https://doi.org/10.1007/s00382-012-1506-x

Roberts, N.M. (2001) Results from simulations of an organised convective event using the New Dynamics at 12, 4 and 2 km resolution. *NWP Technical Report No. 344*. Joint Centre for Mesoscale Meteorology, University of Reading, PO Box 243, Reading, Berkshire RG6 2BB, UK.

Rooney, G.G., Stirling, A.J., Stratton, R.A. & Whitall, M. (2022) C-POOL: a scheme for modelling convective cold pools in the Met Office Unified Model. *Quarterly Journal of the Royal Meteorological Society*, 148, 962–980. Available from: https://doi.org/10.1002/qj.4241

Smith, R.N.B. (1990) A scheme for predicting layer clouds and their water content in a general circulation model. *Quarterly Journal of the Royal Meteorological Society*, 116, 435–460. Available from: https://doi.org/10.1002/qj.49711649210

Tomassini, L., Parker, D.J., Stirling, A., Bain, C., Senior, C. & Milton, S. (2017) The interaction between moist diabatic processes and the atmospheric circulation in African easterly wave propagation. *Quarterly Journal of the Royal Meteorological Society*, 143, 3207–3227. Available from: https://doi.org/10.1002/qj.3173

Walters, D., Baran, A.J., Boutle, I., Brooks, M., Earnshaw, P., Edwards, J. et al. (2019) The Met Office Unified Model global atmosphere 7.0/7.1 and JULES global land 7.0 configurations. *Geoscientific Model Development*, 12(5), 1909–1963. Available from: https://doi.org/10.5194/gmd-12-1909-2019

Whitall, M., Stirling, A., Lock, A., Lavender, S., Stratton, R. & Matsubayashi, K. (2022) The CoMorph convection scheme. UM Documentation Paper 043.

Willett, M.R. & Whitall, M.A. (2017) A simple prognostic based convective entrainment rate for the Unified Model: Description and tests (technical report no. 617). Met Office.

Williams, K.D., Copsey, D., Blockley, E.W., Bodas-Salcedo, A., Calvert, D., Comer, R. et al. (2017) The Met Office global coupled model 3.0 and 3.1 (GC3.0 and GC3.1) configurations. *Journal of Advances in Modeling Earth Systems*, 10, 357–380. Available from: https://doi.org/10.1002/2017MS001115

Wilson, D.R., Bushell, A.C., Kerr-Munslow, A.M., Price, J.D. & Morcrette, C.J. (2008) PC2: a prognostic cloud fraction and condensation scheme. I: scheme description. *Quarterly Journal of the Royal Meteorological Society*, 134, 2093–2107. Available from: https://doi.org/10.1002/qj.333

Wing, A.A., Reed, K.A., Satoh, M., Stevens, B., Bony, S. & Ohno, T. (2018) Radiative–convective equilibrium model intercomparison project. *Geoscientific Model Development*, 11, 793–813. Available from: https://doi.org/10.5194/gmd-11-793-2018

Wing, A.A., Stauffer, C.L., Becker, T., Reed, K.A., Ahn, M.-S., Arnold, N.P. et al. (2020) Clouds and convective self-aggregation in a multimodel ensemble of radiative-convective equilibrium simulations. *Journal of Advances in Modeling Earth Systems*, 12, e2020MS002138. Available from: https://doi.org/10.1029/2020MS002138

Yang, G.Y. & Slingo, J. (2001) The diurnal cycle in the tropics. *Monthly Weather Review*, 129, 784–801.

How to cite this article: Lavender, S.L., Stirling, A.J., Whitall, M., Stratton, R.A., Daleu, C.L., Plant, R.S. *et al*. (2024) The use of idealised experiments in testing a new convective parametrization: Performance of CoMorph-A. *Quarterly Journal of the Royal Meteorological Society*, 150(760), 1581–1600. Available from: https://doi.org/10.1002/qj.4660